305

NAA-SR-1517 (REVISED)
COPY

TWO-GROUP CALCULATIONS OF THE CRITICAL CORE SIZE OF THE SRE REACTOR

AEC Research and Development Report

ATOMICS INTERNATIONAL
A DIVISION OF NORTH AMERICAN AVIATION, INC.

NAA-SR-1517 (REVISED)
PHYSICS AND MATHEMATICS
49 PAGES

TWO-GROUP CALCULATIONS OF THE CRITICAL CORE SIZE OF THE SRE REACTOR

BY
F. L. FILLMORE

ATOMICS INTERNATIONAL
A DIVISION OF NORTH AMERICAN AVIATION, INC.
P.O. BOX 309 CANOGA PARK, CALIFORNIA

CONTRACT: AT(11-1)-GEN-8
ISSUED: JANUARY 15, 1959

ACKNOWLEDGMENT

The author wishes to express his appreciation to J. J. McClure and B. L. Scott for their assistance in performing the calculations described in this report.

DISTRIBUTION

This report has been distributed according to the category "Physics and Mathematics" as given in "Standard Distribution Lists for Unclassified Scientific and Technical Reports" TID-4500 (14th Ed.) October 1, 1958. A Total of 650 copies was printed.

CONTENTS

TABLES

FIGURES

FIGURES (Continued)

ABSTRACT

A brief description of the SRE reactor is given. Basic cross sections and other physical data used in the calculations are listed. The required lattice parameters are evaluated, taking into account the details of the lattice cell structure and core structure. Using two-group reflected reactor theory, the critical mass is calculated for three cases. They are (a) dry: all materials at 20°C and no sodium in the reactor; (b) wet: sodium in the reactor and all materials at 180°C; and (c) hot: operating conditions at full power (20 megawatts) with equilibrium xenon and samarium poison. The value for the effective resonance integral of uranium-238 used in these calculations was obtained from a two-group analysis of uranium graphite exponential experiments. The calculations described in this report are made in a manner consistent with those made for exponential experiments. The flux and adjoint functions in both radial and axial directions are given. The only fuel considered in this study is 2.778 w/o enriched uranium metal.

I. DESCRIPTION OF THE SRE REACTOR

The reactor description given will be sufficient to define the problem but will not contain unnecessary details. A more complete description is given in the book, "Sodium Graphite Reactors."[1]

The core and reflector are composed of hexagonal graphite cells, each 10 feet high and arranged inside a cylindrical stainless-steel tank. Each graphite hexagon is canned in zirconium with 0.035-inch walls. The cans are supported by stainless-steel grids at the top and bottom so that their centers form a triangular lattice with an 11-inch spacing at 20°C. Expansion of the lattice spacing is determined by the temperature of the stainless-steel supports. Figure 1 shows a cross section of a typical cell and of the entire assembly and gives the dimensions of the graphite and zirconium can.

A circular section is removed from a corner of certain cells so that cylindrical passages are formed running the full length of the cells. These passages, which are also shown in Figure 1, are included in the reactor to accommodate thimbles in which control rods, etc. can be placed. There are 17 of these passages fairly uniformly distributed throughout the core. Six of these passages are filled with graphite dummies canned in zirconium, eight with stainless-steel thimbles for control and safety rods, and the remaining three passages with beryllium tubes containing the antimony source, thermocouple wires, and a stainless-steel support. The outside diameter of a stainless-steel thimble is 2-5/8 inches. They are wrapped at an 8-inch pitch with 0.0625-inch stainless-steel wire. The four safety rod thimbles are made of stainless-steel tubing having a 0.035-inch wall; the control rod thimbles have 0.054-inch walls. The interior of the 8 control and safety rod thimbles is assumed to be empty (rods withdrawn).

The fuel is 2.778 w/o enriched uranium metal and is located in process tubes which are coaxial with the graphite cells. There are 43 process tubes which can be loaded with fuel. The loading pattern is shown in Figure 1, and a cross section of the fuel-and-process tube is shown in Figure 2. The fuel is in the form of 3/4-inch rods arranged in a 7-rod cluster. Each rod is clad with a 0.011-inch wall stainless-steel tube which is wrapped at a 12-inch pitch with a 0.091-inch stainless-steel wire. There is a 0.009-inch NaK bond between the cladding and

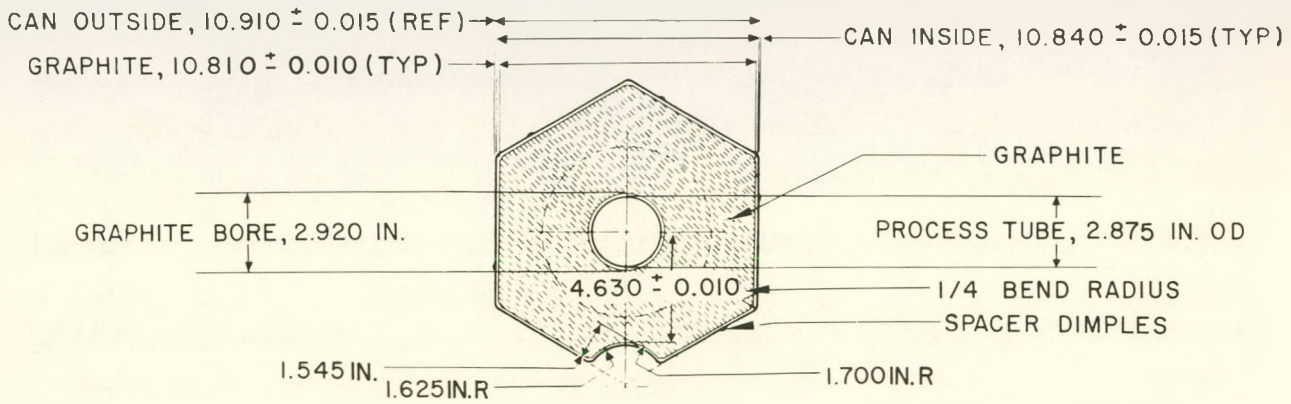

HORIZONTAL CROSS SECTION THROUGH MODERATOR CELL WITH SCALLOPED CORNER WHICH FORMS A PART OF WALL FOR CONTROL AND SAFETY ROD CHANNELS

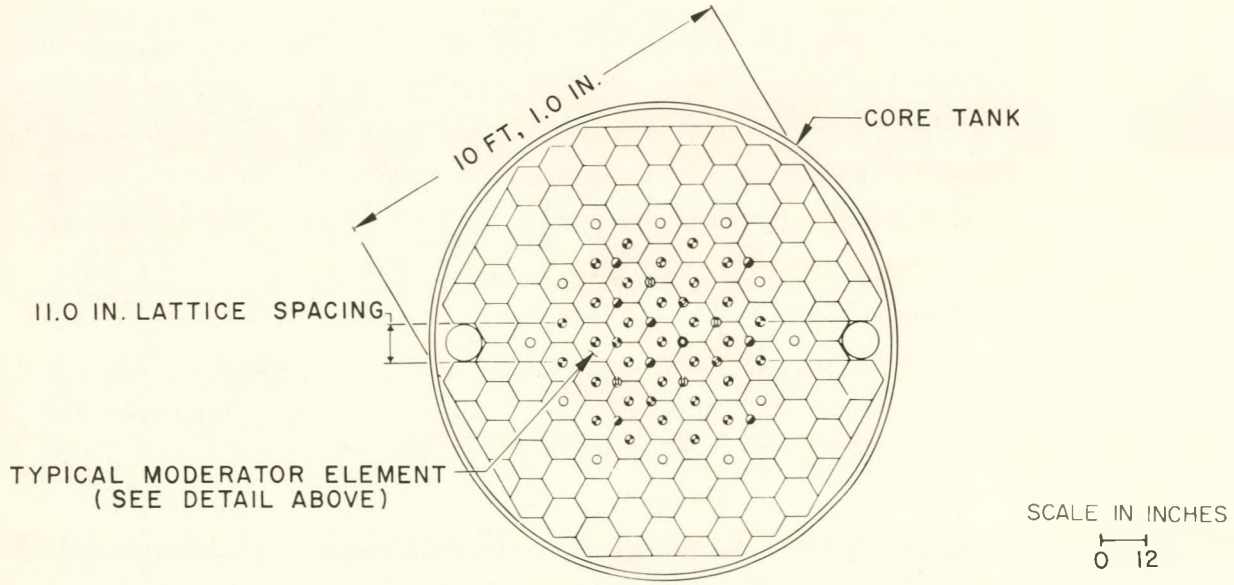

PLAN OF CORE AND REFLECTOR ARRANGEMENT

31	LOADED FUEL CHANNEL
12	EMPTY FUEL CHANNEL FOR INPILE EXPERIMENTS
1	STARTUP NEUTRON SOURCE
8	CHANNEL AVAILABLE FOR TEMPERATURE MEASUREMENT OR EXPERIMENTAL FACILITIES
4	CONTROL ROD
4	SAFETY ROD

Figure 1. Arrangement and Detail of Moderator Cells

the fuel rod at 20°C. As the temperature increases, the fuel expands more the cladding and forces the excess NaK into a reservoir at the top of the fuel rod. The process tube consists of a 2.875-inch-OD zirconium tube having a 0.035-inch wall. The tube is inserted in a bore in the graphite which is 2.920 inches in diameter.

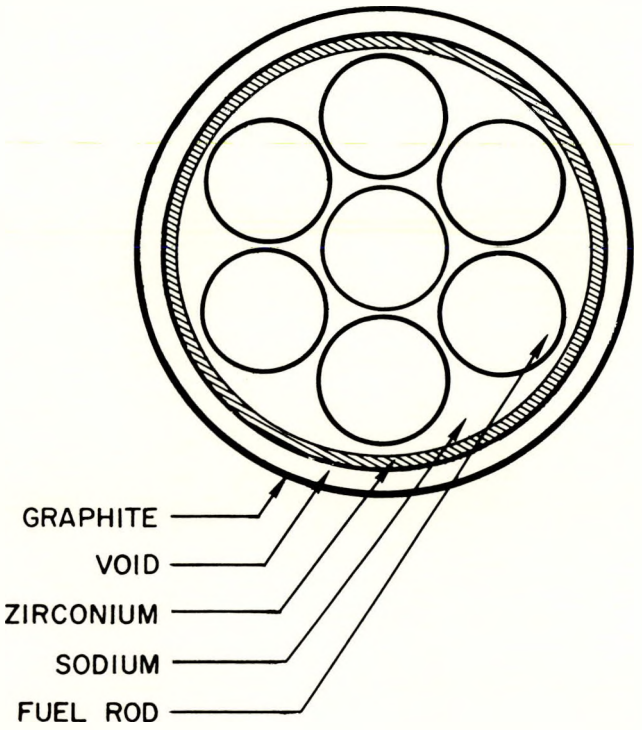

Figure 2. Cross Section of Fuel Cluster and Process Tube

Sodium coolant flows from bottom to top in the process tube and also between the cell cans. It is assumed that the sodium presses the cell cans against the graphite, thus eliminating 90 percent of the void which would otherwise result. The process tube, however, is not distorted by the sodium, so this void remains unaltered. As the temperature rises, the fuel expands more than the process tube, thus reducing the amount of sodium contained therein. Conversely, the cell spacing increases more than the graphite expands, so the amount of sodium between the moderator cans increases. The thickness of the sodium layer between the zirconium cans when they are pressed flat against the graphite is 0.174 inch ± 10 percent at operating temperature. At room temperature this dimension is 0.117 inch ± 10 percent.

The average temperatures of the various materials, when the reactor is in equilibrium at full power (20 megawatts), were estimated by members of the engineering staff. The temperature adopted for each material, the density, and the thermal expansion coefficients are given in Table I.

The cross-sectional area of the stack (core plus reflector) is 12,060 square inches at 20°C, and its height is 10 feet. In calculating the critical size of the core, the stack will be represented by a right circular cylinder having this height and cross section. The resulting height and radius are corrected for thermal expansion, and the extrapolation length, $0.71\lambda_{tr} = 2.13D_{th}$ is added to each boundary. The resulting dimensions, R_0 and H_0 are used in the criticality calculation. The core height, which equals the length of the uranium fuel, is 6 feet at 20°C. This is corrected for thermal expansion, and the result, h_c is used in the criticality calculation to determine the critical mass. These stack dimensions are given in Table II. In the report, "dry" refers to conditions where all materials are at 20°C and there is no sodium in the reactor; "wet" refers to conditions where all materials are at 180°C and sodium is present; and "hot" refers to operating at full power with equilibrium poisons present.

TABLE I

DENSITIES AND THERMAL EXPANSION COEFFICIENTS

Material	Temperature (°C)	Density at 20°C (g/cm^3)	Coefficient of Thermal Expansion per °C
Fuel	500	18.88	37.0×10^{-6} Linear
Graphite	425	1.62	7.8×10^{-6} Linear
Zirconium	400	6.505	6.3×10^{-6} Linear
Stainless Steel	410	7.90	17.3×10^{-6} Linear
Sodium	390	0.8562 (at 390°C)	2.66×10^{-4} Volume
NaK	420	0.906	2.70×10^{-4} Volume

TABLE II

STACK DIMENSIONS

	Dry (cm)	Wet (cm)	Hot (cm)
H_0	308.85	309.25	309.84
R_0	159.27	159.71	160.35
h_c	182.90	183.98	186.15

II. NUCLEAR CROSS SECTIONS AND OTHER DATA

Values for the nuclear cross sections were taken from the AEC compilations[2] and are listed in Tables III through VII. Thermal absorption cross sections are Maxwell averages and are denoted by $\bar{\sigma}$, with the graphite temperature characterizing the Maxwell distribution. No correction was made for neutron spectral hardening because the empirical value of the effective resonance integral used in these calculations was obtained from exponential experiments by means of analysis which contained no spectral hardening.[3] The critical mass calculations described in this report are made in a manner that is consistent with the analysis of the exponential experiments described in Reference 3. All thermal absorption cross sections except $\sigma_a(25)$ and $\sigma_f(25)$ were assumed to have a $1/v$ dependence. The capture-to-fission ratio for uranium-235 was assumed to be constant at the value $\alpha = 0.184$. Except for the fast effect and resonance capture in uranium-238, all epithermal capture and fission was neglected. Cross sections for stainless steel were averaged for a composition of 67 percent iron, 20 percent chromium, 10 percent nickel, 2 percent manganese, and 1 percent silicon. Cross sections for zirconium were averaged for the ingot composition actually being used. No resonance capture was included for zirconium or iron. The graphite cross section results in a thermal diffusion length of 50 cm for graphite of density 1.60 g/cm^3 at 20°C. The composition of NaK is 56 percent sodium and 44 percent potassium by weight.

The equilibrium xenon and samarium poison cross section is given by the following:[4]

$$\Sigma_a(poison) = \Sigma_f(25)\,(1 + \delta)\,(Y_{Sm} + GY_{Xe})$$

$$\delta = \frac{(\epsilon - 1)\nu_{25}}{\nu_{28} - 1} \quad ,$$

where

ϵ = fast fission factor. (Values for ν_{25}, ν_{28} are given in Table VI.)

Y_{Sm} = samarium fission yield = 0.014;

Y_{Xe} = xenon plus iodine fission yield = 0.059;

$G = \bar{\phi}/\{\bar{\phi} + [\lambda_{Xe}/\bar{\sigma}(Xe)]\}$ averaged over the core;

$\bar{\sigma}_a(Xe^{135}) = 2.14 \times 10^6$ barns at 425°C;

λ_{Xe} = xenon decay constant = 2.09×10^{-5} sec^{-1}; and

$\bar{\phi}$ = average flux in the fuel.

The average flux in the fuel is given by the following:

$$\bar{\phi} = \frac{3.12 \times 10^{10}}{\bar{\sigma}_f(25)} \; P \; \frac{238.1 + 235.1E}{E N_0 (\rho V)_{fuel}} = 1.33 \times 10^{13} \; neutrons/cm^2\text{-}sec \; ,$$

where

$E = N_{25}/N_{28}$ = atomic ratio = 0.02893;

P = reactor power = 20×10^6 watts for the hot case and zero for the others;

$(\rho V)_{fuel}$ = mass of fuel; and

N_0 = Avogadro's number.

With $\Sigma_f(25) = 0.393$ cm^{-1} and $G = 0.590$, the following results:

$$\Sigma_a(Poison) = 0.0210 \; cm^{-1} \quad .$$

TABLE III

BASIC MICROSCOPIC CROSS SECTIONS

Material	σ_a (2200) *Barns*	σ_s *Barns*	$\overline{\cos\theta}$	Atomic Weight
Graphite	0.00514	4.8	0.0555	12.00
Uranium 238	2.75	8.3	0.0028	238.1
Uranium 235	687	10	0.0028	235.1
Sodium	0.50	3.5	0.0290	23.00
Zirconium	0.192	8	0.0073	91.22
Stainless Steel	2.94	9.76	0.0117	55.85
Potassium	1.97	1.5	-	39.10

TABLE IV

ADDITIONAL DATA FOR U^{235}*

$\overline{\sigma_f}(20°C)$ = 504.0 barns	$f(20°C)$ = 0.981
$\overline{\sigma_f}(180°C)$ = 396.8 barns	$f(180°C)$ = 0.980
$\overline{\sigma_f}(425°C)$ = 316.0 barns	$f(425°C)$ = 1.002
ν = 2.47 †	

* $\overline{\sigma}$ denotes Maxwell average.

† Number of neutrons per fission.

TABLE V

RESONANCE DATA FOR U^{238}

$$\left(\int_{E_2}^{E_1} \sigma_{res}\,\frac{dE}{E}\right)_{eff} = \frac{7.0}{F} + 29.5\,\frac{S}{M}\ barns \qquad (See\ Reference\ 3)\ .$$

$$F = \frac{\alpha_u r}{2}\,\frac{I_0(\alpha_u r)}{I_1(\alpha_u r)}\ .$$

$\alpha_u = 0.420\ cm^{-1}$

$\sigma_s(fuel) = 8.2\ barns$

$\sigma_s(graphite) = 4.7\ barns$

$\xi(graphite) = 0.1577$ = *average logarithmic-energy decrement per collision*

TABLE VI

MICROSCOPIC URANIUM CROSS SECTIONS AVERAGED OVER THE FISSION SPECTRUM (Barns)

	U^{238}	U^{235}
σ_{total}	7.10	7.1
$\sigma_{fission}$	0.28	1.2
$\sigma_{inelastic}$	1.85	1.5
$\sigma_{capture}$	0.09	0.2
ν	2.5	3.0

TABLE VII

AVERAGE MICROSCOPIC SCATTERING
CROSS SECTIONS FOR FAST NEUTRONS

Material	Cross Section (barns)
Uranium	7.4
Graphite	4.40
Sodium	3.7
Stainless Steel	7.7
Zirconium	8.6
$\bar{\Sigma}_s$(NaK)	0.050 cm^{-1}

III. CELL MODEL AND THERMAL FLUX IN A LATTICE CELL

For the calculation of the thermal utilization and thermal diffusion length, it is necessary to flux-weight the absorption and transport cross sections over the lattice cell. Since no experimental determination of the flux has been made for the SRE lattice cell, a calculation is necessary. Although methods are known for the accurate calculation of the flux, they involve considerable computational labor and are complicated by the structure of the SRE fuel clusters. To avoid these complications, a simple method was used which applied elementary one-group diffusion theory to the five-region model of the lattice cell shown in Figure 3. It is well known that even for a one-coordinate geometry, elementary diffusion theory gives inaccurate results in such calculations. However, flux measurements were available from exponential experiments[3] which had an identical fuel cluster, so that it was possible to estimate the corrections which should be applied to the calculated results. It is believed that the uncertainty introduced into the thermal utilization because of the lack of accurate knowledge about the flux is less than one-half percent.

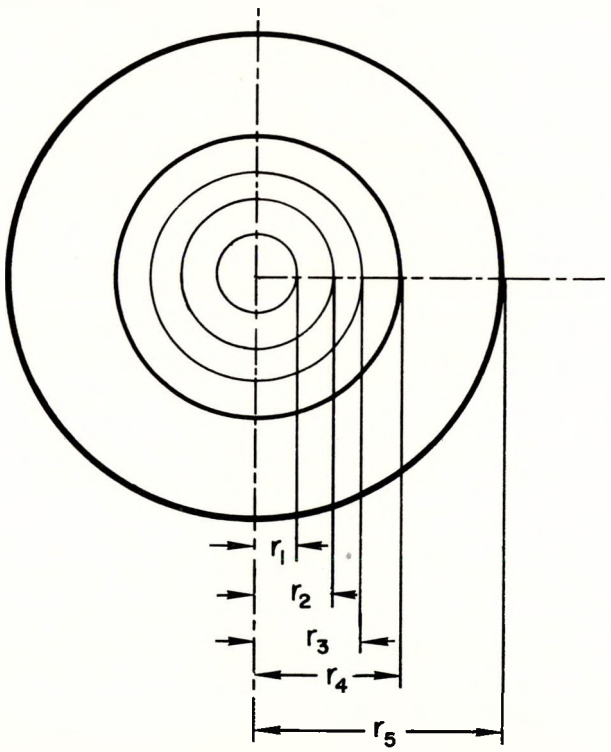

Figure 3. Model Used to Represent 7-Rod Fuel Cluster and Hexagonal Lattice Cell

The cell model used to calculate the flux is shown in Figure 3. The regions are numbered 1 to 5, beginning with the innermost. The boundaries of these regions are determined as follows: r_1 = radius of a fuel rod without its cladding and bond; r_2 and r_3 are determined by requiring that the area of the annulus which they bound shall equal the area of six fuel rods, and that the average of r_2 and r_3 shall equal the radius of the circle upon which the centers of the six outer fuel rods are located; r_4 is the radius of the graphite bore; and r_5 is the radius of a circle whose area equals that of the hexagonal cell. Values of these radii are given in Table VIII.

TABLE VIII

DIMENSIONS AND NUCLEAR DATA FOR THE CELL MODEL

Region		r_i (cm)			Σ_a (cm^{-1})		
		Dry	Wet	Hot	Dry	Wet	Hot
1		0.9520	0.9577	0.9689	0.8975	0.6960	0.5586
2		1.671	1.662	1.649	-	0.03431	0.02763
3		2.869	2.875	2.890	0.8975	0.6960	0.5560
4		3.708	3.712	3.719	-	0.01480	0.01480
5		14.670	14.710	14.764	3.706×10^{-4}	2.971×10^{-4}	2.379×10^{-4}
Region	$\cos\theta$	Σ_{tr} (cm^{-1})			$\mathscr{H}$ (cm^{-1})		
		Dry	Wet	Hot	Dry	Wet	Hot
1	0.0028	1.2951	1.0865	0.9325	1.292	1.079	0.8969
2	0.0290	-	0.2281	0.2221	-	0.1419	0.1269
3	0.0028	1.2951	1.0865	0.9325	1.292	1.079	0.8969
4	0.0290	-	0.1577	0.1548	-	0.07930	0.07103
5	0.0555	0.3691	0.3677	0.3655	0.02025	0.1810	0.01615

It was assumed that regions 1 and 3 consist only of fuel; region 5, only of graphite; region 2, of a homogeneous mixture in the proper ratios of sodium, potassium, and stainless steel; and region 4, of a homogeneous mixture of sodium, stainless steel and zirconium. If the sodium is removed from the cell as in the dry case, it is assumed that the flux is constant in regions 2 and 4. Average

thermal absorption and transport cross sections for each region were calculated and are also listed in Table VIII. Table IX gives the macroscopic cross sections for each material.

TABLE IX

MACROSCOPIC MATERIAL CROSS SECTIONS
AVERAGED OVER A MAXWELL FLUX DISTRIBUTION

Material	Dry		Wet		Hot	
	Absorption Cross Section (cm^{-1})	Transport Cross Section (cm^{-1})	Absorption Cross Section (cm^{-1})	Transport Cross Section (cm^{-1})	Absorption Cross Section (cm^{-1})	Transport Cross Section (cm^{-1})
Fuel	0.9223	1.3061	0.7225	1.1068	0.5695	0.9740
NaK	0.01484	0.06391	0.01194	0.06080	0.009614	0.05814
Stainless Steel	0.2222	1.0442	0.1772	0.9925	0.1410	0.9465
Sodium	-	-	0.008484	0.08933	0.006441	0.08266
Zirconium	0.007313	0.3486	0.005868	0.3461	0.004709	0.3435
Graphite	0.0003706	0.3691	0.0002971	0.3677	0.0002379	0.3655

The inverse thermal diffusion length and thermal diffusion coefficient for each region were calculated from the following formulas:

$$\frac{\kappa}{\Sigma_a + \Sigma_s} = \tanh \frac{\kappa}{\Sigma_s} \quad (\textit{regions } 1 \textit{ and } 3) \ .$$

$$\kappa^2 = 3\Sigma_{tr}\Sigma_a \left[1 - \frac{4}{5}\frac{\Sigma_a}{\Sigma_s + \Sigma_a}\right] \quad (\textit{regions } 2, 4, \textit{ and } 5) \ .$$

$$D_{th} = \frac{\Sigma_a}{\kappa^2}$$

$$\Sigma_{tr} = \Sigma_s(1 - \overline{\cos\theta}) + \Sigma_a \ .$$

The absorption cross sections for the hot case (operation at full power) include equilibrium samarium and xenon poison.

The desired solution of the one-group diffusion equation for an infinitely long cylinder is of the following form:

$$\phi_i(r) = A_i I_0(\kappa_i r) + B_i K_0(\kappa_i r) + \frac{Q_i}{\kappa_i^2 D_i} \qquad r_i - 1 \leq r \leq r_i \ ,$$

where

i = 1, 2, 3, 4, 5 refers to the regions shown in Figure 3;

κ_i = inverse diffusion length in i^{th} medium;

D_i = diffusion coefficient in i^{th} medium; and

Q_i = source in i^{th} region, which is taken to be zero in regions 1 to 4, and constant in region 5.

I_0 and K_0 are modified Bessel Functions, and A_i and B_i are constants which are determined by the boundary conditions. The condition that the flux be finite at $r = 0$ requires that $B_1 = 0$ and the flux was normalized so that $A_1 = 1$. The neutron current vanishes at the cell boundary, $r = r_5$, which requires that

$$B_5 = A_5 \frac{I_1(\kappa_5 r_5)}{K_1(\kappa_5 r_5)} \ .$$

The continuity of flux and current at the interface leads to the following matrix equations for the remaining constants:

$$\begin{pmatrix} A_{i+1} \\ \\ B_{i+1} \end{pmatrix} = \kappa_{i+1} r_i \begin{pmatrix} K_1 & K_0 \\ \kappa_{i+1} r_i & \\ I_1 & -I_0 \end{pmatrix} \begin{pmatrix} 1 & 0 \\ \\ 0 & \dfrac{D_i \kappa_i}{D_{i+1} \kappa_{i+1}} \end{pmatrix} \begin{pmatrix} I_0 & K_0 \\ \kappa_i r_i & \\ I_1 & -K_1 \end{pmatrix} \begin{pmatrix} A_i \\ \\ B_i \end{pmatrix} \ ,$$

where

$i = 1, 2, 3$; and

$$\begin{pmatrix} A_5 \\ \dfrac{Q_5}{\aleph_5^2 D_5} \end{pmatrix} = \frac{1}{Y_{4,5}} \begin{pmatrix} 0 & -K_1(\aleph_5 r_5) \\ Y_{4,5} & -W_{4,5} \end{pmatrix} \begin{pmatrix} 1 & 0 \\ 0 & \dfrac{D_4 \aleph_4}{D_5 \aleph_5} \end{pmatrix} \begin{pmatrix} I_0 & K_0 \\ I_1 & -K_1 \end{pmatrix} \begin{pmatrix} A_4 \\ B_4 \end{pmatrix} \quad \aleph_4 r_4 .$$

The expression $\aleph_i r_i$ in the center of a matrix is the argument of each Bessel function in that matrix. The W's and Y's are defined as follows:

$$W_{4,5} = \begin{vmatrix} I_0(\aleph_5 r_4) & K_0(\aleph_5 r_4) \\ I_1(\aleph_5 r_5) & -K_1(\aleph_5 r_5) \end{vmatrix}$$

and

$$Y_{4,5} = \begin{vmatrix} I_1(\aleph_5 r_4) & -K_1(\aleph_5 r_4) \\ I_1(\aleph_5 r_5) & -K_1(\aleph_5 r_5) \end{vmatrix} .$$

The average flux in the i^{th} region is given by the following:

$$\bar{\phi}_i = \frac{2\pi\psi_i}{V_i} ,$$

where

V_i = the volume of the i^{th} region, and

$$\psi_i = \frac{A_i}{\aleph_i} \left[r I_1(\aleph_i r) \right]_{r_{i-1}}^{r_i} - \frac{B_i}{\aleph_i} \left[r K_1(\aleph_i r) \right]_{r_{i-1}}^{r_i} + \frac{Q_i}{2\aleph_i^2 D_i} \left[r_i^2 - r_{i-1}^2 \right] .$$

Figure 4 shows a graph of the flux in a cell as calculated by the aforementioned method. Table X gives the computed values of the average flux, $\bar{\phi}_i$ and $\bar{\phi}(r_i)$, together with their corrected values. The corrected values were obtained by applying to the calculated values, experimentally determined correction factors which were obtained from the flux measurements in the exponential experiments.[3] A control rod type of calculation indicated that the average flux in the stainless-steel thimbles should be reduced by a factor of 0.945 from the corrected value.

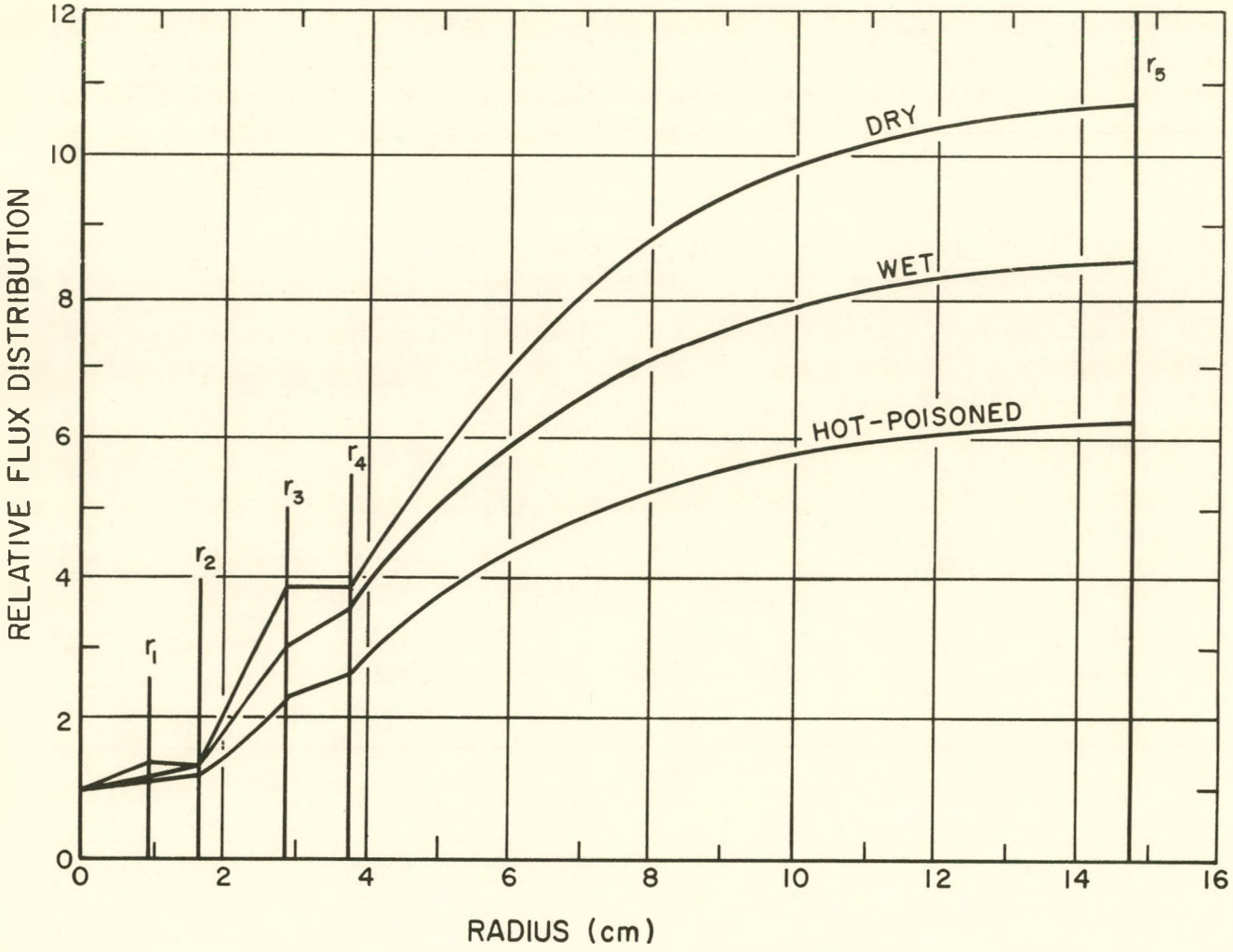

Figure 4. Calculated Flux in Lattice Cell Model

The volume fractions of each material in the cell were calculated, assuming the materials in the thimbles to be uniformly distributed throughout the core.

For this purpose the core size was assumed to be 22, 31, and 37 cells for the dry, wet, and hot cases, respectively. Table XI gives the results. It should be noted that the volume fraction of several of the materials is divided into more than one part. This is done so that the flux variation in the cell may be applied properly in calculating cell averaged cross sections.

TABLE X

AVERAGE FLUX IN CELL

	Calculated Flux			Adjustment Factor	Adjusted Flux		
	Dry	Wet	Hot		Dry	Wet	Hot
$\bar{\phi}_1$	1.202	1.140	1.097	1.00	1.202	1.140	1.097
$\phi(r_1)$	1.416	1.285	1.198	1.03	1.458	1.324	1.234
$\bar{\phi}_2$	1.416	1.353	1.238	1.03	1.458	1.394	1.275
$\phi(r_2)$	1.416	1.409	1.291	1.03	1.458	1.451	1.329
$\bar{\phi}_3$	2.297	2.095	1.739	1.04	2.493	2.178	1.808
$\phi(r_3)$	3.856	3.061	2.344	1.07	4.126	3.275	2.508
$\bar{\phi}_4$	3.856	3.309	2.501	1.20	4.627	3.971	3.001
$\phi(r_4)$	3.856	3.547	2.672	1.30	5.013	4.611	3.474
$\bar{\phi}_5$	9.517	7.035	5.286	1.21	11.515	8.513	6.396
$\phi(r_5)$	10.742	8.491	6.208	1.23	13.213	10.443	7.636

TABLE XI

VOLUME FRACTIONS FOR EACH MATERIAL IN A CORE CELL

Region	Material	Volume Fraction		
		Dry	Wet	Hot
1	Fuel 1 rod	0.004211	0.004329	0.004307
2	NaK bond 1 rod	0.000216	0.000188	0.000116
	Stainless steel 1 rod	0.000322	0.000322	0.000322
	Sodium (void for dry case)	0.006502	0.006460	0.006415
	Stainless steel portion of 6 rods	0.000965	0.000965	0.000965
	NaK bond portion of 6 rods	0.000649	0.000563	0.000349
3	Fuel 6 rods	0.025268	0.025432	0.025840
4	NaK bond portion of 6 rods	0.000649	0.000563	0.000349
	Stainless steel portion of 6 rods	0.000965	0.000965	0.000965
	Sodium (void for dry core)	0.019015	0.018983	0.018849
	Zirconium process tube	0.002980	0.002969	0.002955
	Void at process tube wall	0.002056	0.002029	0.002020
5	Graphite	0.870189	0.86960	0.864598
	Void in thimbles and between graphite and can	0.016400	0.014110	0.015956
	Zirconium-moderator can and thimbles	0.014388	0.014338	0.014269
	Sodium (void for dry case) between can and in thimble channels	0.034486	0.037247	0.040855
	Stainless steel in thimbles	0.001581	0.001122	0.000940

IV. FORMULAS FOR CALCULATING THE LATTICE CONSTANTS

A. CROSS SECTIONS

The absorption and transport cross sections, flux-averaged over the unit cell are given by the following:

$$\bar{\Sigma} = \frac{\sum_i \bar{\phi}_i V_i \Sigma_i}{\sum_i \bar{\phi}_i V_i} \quad ,$$

where

V_i represents the volume fractions and the summation is over all materials in the cell, including the void.

B. THERMAL UTILIZATION

$$f = \frac{(\bar{\phi}_1 V_1 + \bar{\phi}_3 V_3)\, \Sigma_a(fuel)}{\sum_i \bar{\phi}_i V_i \Sigma_{ai}} \quad .$$

C. THERMAL DIFFUSION LENGTH

$$L^2 = \frac{1}{3\bar{\Sigma}_a \bar{\Sigma}_{tr}} \, .$$

D. RESONANCE ESCAPE PROBABILITY

$$p = e^{-1/G} \quad ,$$

where

$$G = \frac{\textit{neutrons removed from the resonance energy by slowing down in the moderator}}{\textit{resonance neutrons absorbed in the fuel}} \quad .$$

The formula for G is taken to be the following:

$$G = \frac{V_m (\xi \Sigma_s)_m}{V_u N_u \left(\int \sigma_{res} \frac{dE}{E} \right)_{eff}} \quad ,$$

where the subscript m refers to moderator and u refers to fuel. The value used for the effective resonance integral with the $1/v$ absorption tail removed[3] was as follows:

$$\left(\int \sigma_{res} \frac{dE}{E} \right)_{eff} = \frac{7.0}{F} + 29.5 \frac{S}{M} \textit{ barns} \quad .$$

F is the disadvantage factor of the seven fuel rods for the resonance neutrons and was taken to be the following:

$$F = \frac{\varkappa_u r_1 \sqrt{7}}{2} \frac{I_0(\varkappa_u r_1 \sqrt{7})}{I_1(\varkappa_u r_1 \sqrt{7})} \quad .$$

The data used are given in Table V.

The S/M term in the effective resonance integral was calculated, as suggested by Dr. E. R. Cohen, by taking the surface to be that given by placing a taut rubber band around the outside of the fuel rods. This is the proper surface to use, provided that a neutron which enters the region inside this surface cannot escape without traversing a fuel rod. This is the case for the fuel cluster if scattering in the sodium is neglected.

Correction to p for the doppler broadening of the resonances due to a temperature of T°C was taken to be the following:[5]

$$p(T) = p_{20°C} \exp\left\{-\frac{1}{G}\left[1.3 \times 10^{-4}\,(T - 20°C)\right]\right\} \quad .$$

E. ETA

$$\eta = \frac{\nu\bar{\sigma}_f(25)}{\bar{\sigma}_a(25) + \frac{1}{E}\bar{\sigma}_a(28) + \frac{\Sigma_a(poison)}{N_{25}}} \quad .$$

F. EPSILON

$$\epsilon = 1 + \frac{[(\nu - 1)\sigma_f - \sigma_c]P}{\sigma_t - [\nu\sigma_f + \sigma_e]P} \quad ,$$

where the cross sections are averaged over the fission spectrum and

$$\sigma_t = \sigma_c + \sigma_f + \sigma_{in} + \sigma_e \quad .$$

These cross sections are for the enriched fuel and are given by the following:

$$\sigma_{fuel} = \frac{E}{1 + E}\sigma_{25} + \frac{E}{1 + E}\sigma_{28} \quad .$$

P is the first collision probability for a fission neutron in the fuel cluster and is obtained from the curves by Garvey,[6] which give P for hollow cylinders. The hollow cylinder used here is region 3 of Figure 3, with the inner fuel rod distributed uniformly on the inside of the region. The variation of ϵ with temperature was found to be negligible.

G. AGE

$$\tau = [\tau_f - (\tau_f - \tau_{in}) \frac{\sigma_{in} P}{\sigma_{tot}} + \frac{D}{(\xi \Sigma_s)_m} \ln \frac{1.44}{5kT} \left(\frac{\rho_0}{\rho}\right)^2 \frac{1}{V_m(1 - V_0)} \quad ,$$

where

τ_f = age in graphite of fission neutrons to the indium resonance;

τ_{in} = age in graphite of inelastically scattered fission neutrons to the indium resonance;

P = collision probability for fission neutrons in the fuel cluster;

ρ = graphite density;

V_0 = volume fraction of void;

$V_m = \sum_i V_i \frac{(\xi \Sigma_s)_i}{(\xi \Sigma_s)_{graphite}}$, where the summation is over all the cell; and

$\frac{D}{\xi \Sigma_s}$ = 15.01 for epithermal neutrons in graphite of density 1.60 g/cm^3.

The correction of the age from the indium resonance to thermal energy is made to the energy 5kT.[7]

H. FAST NEUTRON TRANSPORT CROSS SECTIONS

Fast neutron absorption was neglected, and it was assumed that the average fast neutron flux was constant over the cell so that no flux weighting of the cross sections was required.

$$\bar{\Sigma}_{tr} = \sum_i V_i (1 - \overline{\cos \theta_i}) \Sigma_s(i) \quad ,$$

where $\overline{\cos \theta}$ is the average cosine of the scattering angle in the laboratory system. The values used for the average scattering cross section for fast neutrons are

listed in Table VII. The temperature dependence of $\bar{\Sigma}_{tr}$ was assumed to be the same as for graphite, namely $(1 - 3\alpha_{gr}\Delta T)$.

The diffusion coefficient for fast neutrons is as follows:

$$D_f = \frac{1}{3\bar{\Sigma}_{tr}} ,$$

and the slowing down cross section for the cell is

$$\Sigma_{sl} = \frac{D_f}{\tau} .$$

I. STREAMING CORRECTION

Because of the significant amount of voids present in the reactor for the dry case where no sodium is present, it is necessary to correct the age and thermal diffusion length for neutron streaming. The following formula was used.[8]

$$\left(\frac{\Lambda}{\Lambda_0}\right)^2 = \prod_{i=1}^{n} \left[1 + 2H_i + \frac{H_i^2 \left(\frac{2r_i}{H_i\lambda}\right)}{exp\left(\frac{2r_i}{H_i\lambda}\right) - 1} + \frac{r_i H_i Q_i}{\lambda} \right] \frac{1}{(1 + H_T)^2} ,$$

where

H_i = the ratio of the volume per cell of the i^{th} void to the total volume of material;

r_i = the hydraulic radius of the i^{th} void defined as the cross section area divided by the perimeter;

λ = the transport mean free path in graphite;

Q = a factor which depends upon the shape of the void;

$H_T = \sum_{i=1}^{n} H_i$;

and

n = number of voids per unit cell.

The quantity in the brackets corrects for the effect of a single void through a solid, and the effect of these voids must be multiplied together. In the calculation of the quantity Λ_0^2, to which the streaming correction is applied, the void was homogenized over the lattice cell. Because of this, the factor $1/(1 + H_T)^2$ is required to reduce Λ_0^2 to its appropriate value for use in the Behrens formula. Application of this procedure gave the value $(\Lambda/\Lambda_0)^2 = 1.072$ for the neutron streaming correction in the core.

V. SUMMARY OF CALCULATED RESULTS FOR THE LATTICE

The results of the lattice calculations which were outlined in the preceding section are given in Table XII. The buckling listed is the positive value of B^2 calculated from the following two-group formula:

$$(1 + \tau B^2)(1 + L^2 B^2) = k_\infty \quad .$$

TABLE XII

CORE DATA

Parameter	Dry	Wet	Hot
η	1.8274	1.8231	1.7527
ϵ	1.0433	1.0433	1.0433
f	0.8502	0.8140	0.8403
p	0.8193	0.8159	0.8091
k_∞	1.3280	1.2631	1.2433
$\Sigma_a(cm^{-1})$	0.006604	0.006528	0.005661
$L^2(cm^2)$	154.8	148.1	173.1
$D_{th}(cm)$	1.022	0.9598	0.9726
$\tau(cm^2)$	425.0	371.3	370.4
$D_f(cm)$	1.140	1.077	1.088
$B^2(cm^{-2})$	0.0005334	0.0004820	0.0004262

VI. REFLECTOR

The radial and axial reflectors must be treated separately because of the different geometries and materials involved. The radial reflector was divided into two regions. The outer region consists entirely of solid-graphite hexagons, whose dimensions were identical with those used in the core and are canned in zirconium as are those in the core. The inner region contained cells which had fuel channels that were filled with graphite dummies instead of fuel together with 18 of the solid-graphite cells. D_{th}, L^2, τ, and D_f were then calculated for each section according to the same method used in the core, except that no flux weighting was applied. The final radial reflector was then a composite of these two regions obtained by weighting the regions in proportion to the square of the macroscopic neutron flux in the reflector. The flux used was obtained from previous SRE calculations.[9] The properties of the radial reflector are shown in Table XIII.

TABLE XIII

RADIAL REFLECTOR DATA

Parameter	Dry	Wet	Hot
$D_{th}(cm)$	0.9854	0.9299	0.9396
$L^2(cm^2)$	2163.	1467.	1836.
$\tau(cm^2)$	367.0	338.3	336.1
$D_f(cm)$	1.056	1.0133	1.0215

The properties of the axial reflector are more difficult to evaluate because of the more complicated geometry and the lack of symmetry between the top and bottom reflectors. What is desired is an average homogeneous reflector which has the same effect on reactivity as have the top and bottom reflectors combined. The reflector constants were obtained in the same manner as those for the radial reflector except that here the reflector was divided into five sections: two at the top and three at the bottom. The composite reflector is an average of the

five sections weighted by the square of the flux. The properties of the axial reflector which is now assumed to be symmetrically distributed, are shown in Table XIV.

TABLE XIV

AXIAL REFLECTOR DATA

Parameter	Dry	Wet	Hot
$D_{th}(cm)$	1.079	0.9787	0.9911
$L^2(cm^2)$	605.9	553.4	669.8
$\tau(cm^2)$	478.7	383.7	378.0
$D_f(cm)$	1.205	1.110	1.122

VII. THE TWO-GROUP CRITICALITY PROBLEM

In attempting to solve the two-group, two-region boundary value problem using the method of separation of variables in cylindrical coordinates for a reactor reflected axially as well as radially, it is found that the boundary conditions at all points of the core-reflector boundary are not satisfied by the fundamental mode solution. Therefore, this well-known method fails in this case. However, an approximate solution can be obtained by treating the radial problem as a cylindrical reactor which is reflected radially but is bare on the ends, and the axial problem as a cylindrical reactor which is reflected on the ends but is bare radially. The material buckling is found by solving the following characteristic equation:

$$(1 + L^2B^2)(1 + \tau B^2) = k_\infty \quad .$$

The buckling is then divided into radial and axial components as follows:

$$B^2 = B_r^2 + B_z^2 \quad .$$

It is desired to find the core volume which will make the reactor critical. Since the height of the core and the height and radius of the stack are given, the parameters to be adjusted to produce criticality are the axial buckling and the core radius. The axial problem is solved first by assuming a value for B_r^2 and finding the core height (h) which produces criticality. If this calculated value of h is not equal to the actual core height, another value of B_r^2 is tried and the calculation repeated. This procedure can be continued until the calculated value of h is equal to the actual core height. The radial problem is then solved for the critical radius of the core (R_c), using the axial buckling corresponding to the correct core height.

It is actually not necessary to continue the solution of the axial problem until h is exactly equal to the core height, because if h is close to the actual

height, the critical volume of the core will be given to sufficient accuracy by $\pi R_c^2 h$. Since the volume of a cell is known, the number of cells which must be loaded can then be found. The thermal and fast fluxes and the adjoint functions are evaluated next, and if h is within one or two centimeters of the actual height, they will be given with sufficient accuracy for use in perturbation theory calculations.

The equations used in solving the two-group, two-region problems follow. Subscripts 1 and 2 refer to fast and thermal neutrons, respectively; subscripts c and 0 refer to core and reflector, respectively. The two roots of the characteristic equation are μ^2 and $-\nu^2$

A. AXIAL FLUX

$$\phi_{1c} = A \cos B_z z + C \cosh \gamma z \quad ; \qquad 0 \le |z| \le h/2 \quad ;$$

$$\phi_{2c} = AS_c \cos B_z z + CT_c \cosh \gamma z \quad ;$$

$$\phi_{10} = F \sinh \varkappa_{10} \left(\frac{H_0}{2} - z \right) \quad ; \qquad h/2 \le |z| \le \frac{H_0}{2} \quad ;$$

$$\phi_{20} = FS_0 \sinh \varkappa_{10} \left(\frac{H_0}{2} - z \right) + G \sinh \varkappa_{20} \left(\frac{H_0}{2} - z \right) ;$$

where

$$\gamma^2 = \mu^2 + \nu^2 - B_z^2 \quad ;$$

$$\varkappa_{10}^2 = \frac{1}{\tau_0} + B_r^2 \quad ;$$

$$\varkappa_{20}^2 = \frac{1}{L_0^2} + B_r^2 \quad ;$$

$$S_c = \frac{p_c D_{1c}}{\tau_c D_{2c}} \frac{1}{\frac{1}{L_c^2} + \mu^2} \quad ;$$

$$T_c = \frac{p_c D_{1c}}{\tau_c D_{2c}} \frac{1}{\frac{1}{L_c^2} - \nu^2} \quad ;$$

$$S_0 = \frac{D_{10}}{\tau_0 D_{20}} \quad \frac{1}{\kappa_{20}^2 - \kappa_{10}^2} \quad .$$

The criticality equation is as follows:

$$\begin{vmatrix} \cos B_z \frac{h}{2} & \cosh \gamma \frac{h}{2} & -\sinh \kappa_{10} \frac{H_0 - h}{2} & 0 \\ -D_{1c} B_z \sin B_z \frac{h}{2} & D_{1c} \gamma \sinh \gamma \frac{h}{2} & D_{10} \kappa_{10} \cosh \kappa_{10} \frac{H_0 - h}{2} & 0 \\ S_c \cos B_z \frac{h}{2} & T_c \cosh \gamma \frac{h}{2} & -S_0 \sinh \kappa_{10} \frac{H_0 - h}{2} & -\sinh \kappa_{20} \frac{H_0 - h}{2} \\ -D_{2c} S_c B_z \sin B_z \frac{h}{2} & D_{2c} T_c \gamma \sinh \gamma \frac{h}{2} & D_{20} S_0 \kappa_{10} \cosh \kappa_{10} \frac{H_0 - h}{2} & D_{20} \kappa_{20} \cosh \kappa_{20} \frac{H_0 - h}{2} \end{vmatrix} = 0 \ .$$

B. AXIAL ADJOINT FUNCTIONS

$$\phi_{1c}^* = A^* \cos B_z z + C^* \cosh \gamma z \quad ;$$

$$\phi_{2c}^* = A^* S_c^* \cos B_z z + C^* T_c^* \cosh \gamma z \quad ; \qquad 0 \le |z| \le \frac{h}{2} \quad ;$$

$$\phi_{10}^* = G^* T^* \sinh \kappa_{20} \left(\frac{H_0}{2} - z \right) + F^* \sinh \kappa_{10} \left(\frac{H_0}{2} - z \right) \quad ;$$

$$\phi_{20}^* = G^* \sinh \kappa_{20} \left(\frac{H_0}{2} - z \right) \quad ; \qquad \frac{h}{2} \le |z| \le \frac{H_0}{2} \quad ;$$

where

$$S_c^* = \frac{1 + \tau_c \mu^2}{p_c} \quad ;$$

$$T_c^* = \frac{1 - \tau_c \nu^2}{p_c} \quad ;$$

$$T_0^* = \frac{1}{\tau_0 (\kappa_{10}^2 - \kappa_{20}^2)} \quad .$$

C. RADIAL FLUX

$$\phi_{1c} = \bar{A} J_0(\alpha r) + \bar{C} J_0(\beta r) \quad ;$$

$$0 \leq r \leq R_c \quad ;$$

$$\phi_{2c} = \bar{A} S_c J_0(\alpha r) + \bar{C} T_c I_0(\beta r) \quad ;$$

$$\phi_{10} = \bar{F} Z(\kappa_{10}, r) \quad ;$$

$$R_c \leq r \leq R_0 \quad ;$$

$$\phi_{20} = \bar{F} S_0 Z(\kappa_{10}, r) + \bar{G} Z(\kappa_{20}, r) \quad ;$$

where

$$\alpha^2 = \mu^2 - B_z^2 \quad ;$$

$$\beta^2 = \nu^2 + B_z^2 \quad ;$$

$$Z(\kappa, r) = I_0(\kappa r) - \frac{I_0(\kappa R_0)}{K_0(\kappa R_0)} K_0(\kappa r) \quad ;$$

$$\kappa_{10}^2 = \frac{1}{\tau_0} + B_z^2 \quad ;$$

$$\kappa_{20}^2 = \frac{1}{L_0^2} + B_z^2 \quad .$$

The criticality equation is as follows:

$$\begin{vmatrix} J_0(\alpha R) & I_0(\beta R) & -Z(\kappa_{10}, R) & 0 \\ -D_{1c}\alpha J_1(\alpha R) & D_{1c}\beta I_1(\beta R) & -D_{10} Z'(\kappa_{10}, R) & 0 \\ S_c J_0(\alpha R) & T_c I_0(\beta R) & -S_0 Z(\kappa_{10}, R) & -Z(\kappa_{20}, R) \\ -D_{2c} S_c \alpha J_1(\alpha R) & D_{2c} T_c \beta I_1(\beta R) & -D_{20} S_0 Z'(\kappa_{10}, R) & -D_{20} Z'(\kappa_{20}, R) \end{vmatrix} = 0 \quad .$$

D. RADIAL ADJOINT FUNCTIONS

$$\phi_{1c}^{*} = \bar{A}^{*} J_0(\alpha r) + \bar{C}^{*} I_0(\beta r) \quad ; \qquad 0 \le r \le R_c \quad ;$$

$$\phi_{2c}^{*} = \bar{A}^{*} S_c^{*} J_0(\alpha r) + \bar{C}^{*} T_c^{*} I_0(\beta r) \quad ;$$

$$\phi_{10}^{*} = \bar{G}^{*} T_0^{*} Z(\mathscr{K}_{20}, r) + \bar{F}^{*} Z(\mathscr{K}_{10}, r) \quad ; \qquad R_c \le r \le R_0 \quad ;$$

$$\phi_{20}^{*} = \bar{G}^{*} Z(\mathscr{K}_{20}, r) \quad .$$

VIII. RESULTS

The critical volume was calculated for each of the three cases under consideration, and the number of cells required to give this volume was then determined. The results are given in Table XV.

TABLE XV

RESULTS OF CRITICAL CALCULATIONS

	Calculated Mass of U^{235} (kg)	Calculated Core Volume (cm^3)	Calculated No. of Cells	Experimental No. of Cells	Error (%)
Dry	48.79	3.154×10^6	25.5	22.2	14.9
Wet	70.71	4.595×10^6	36.7	32.7	11.9
Hot	89.28	5.844×10^6	45.9	-	-

The flux and adjoint functions were calculated for each case. The results, normalized to unit thermal flux at the center of the reactor, are shown in Figures 5, 6, and 7 for the axial case and in Figures 8, 9, and 10 for the radial.

The average value of the thermal flux over the core was calculated by normalizing the flux $\phi_{2c}(r, z) = \phi_{2c}(r)\phi_{2c}(z)$ to unity at the center of the core and then evaluating the following expression:

$$\bar{\phi}_c = \frac{2\pi}{\pi R_c^2 H_c} \int_{core} \phi_{2c}(r)\phi_{2c}(z)\, r dr dz \quad .$$

The result for the hot case is as follows:

$$\frac{\bar{\phi}_c}{\phi_{2c}(0, 0)} = 0.595 \quad .$$

The ratio of the peak to average flux along the z axis is 1.240.

In calculating the axial and radial problems it must be remembered that the properties of the outer region have different values in each case. Although the formula for S_0 and T_0^* are the same in both cases, their numerical values are not.

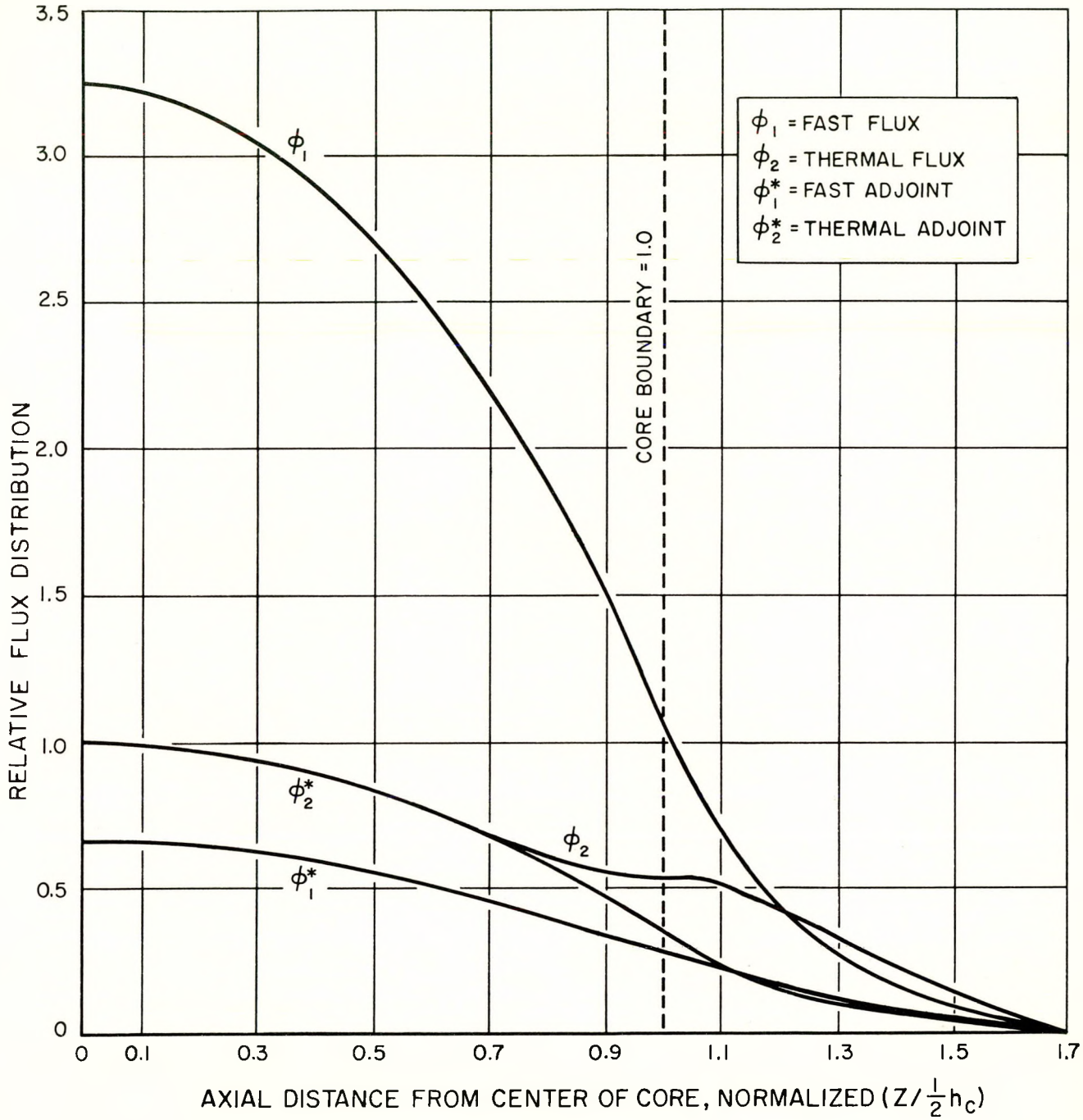

Figure 5. Axial Flux Plot for Dry Case

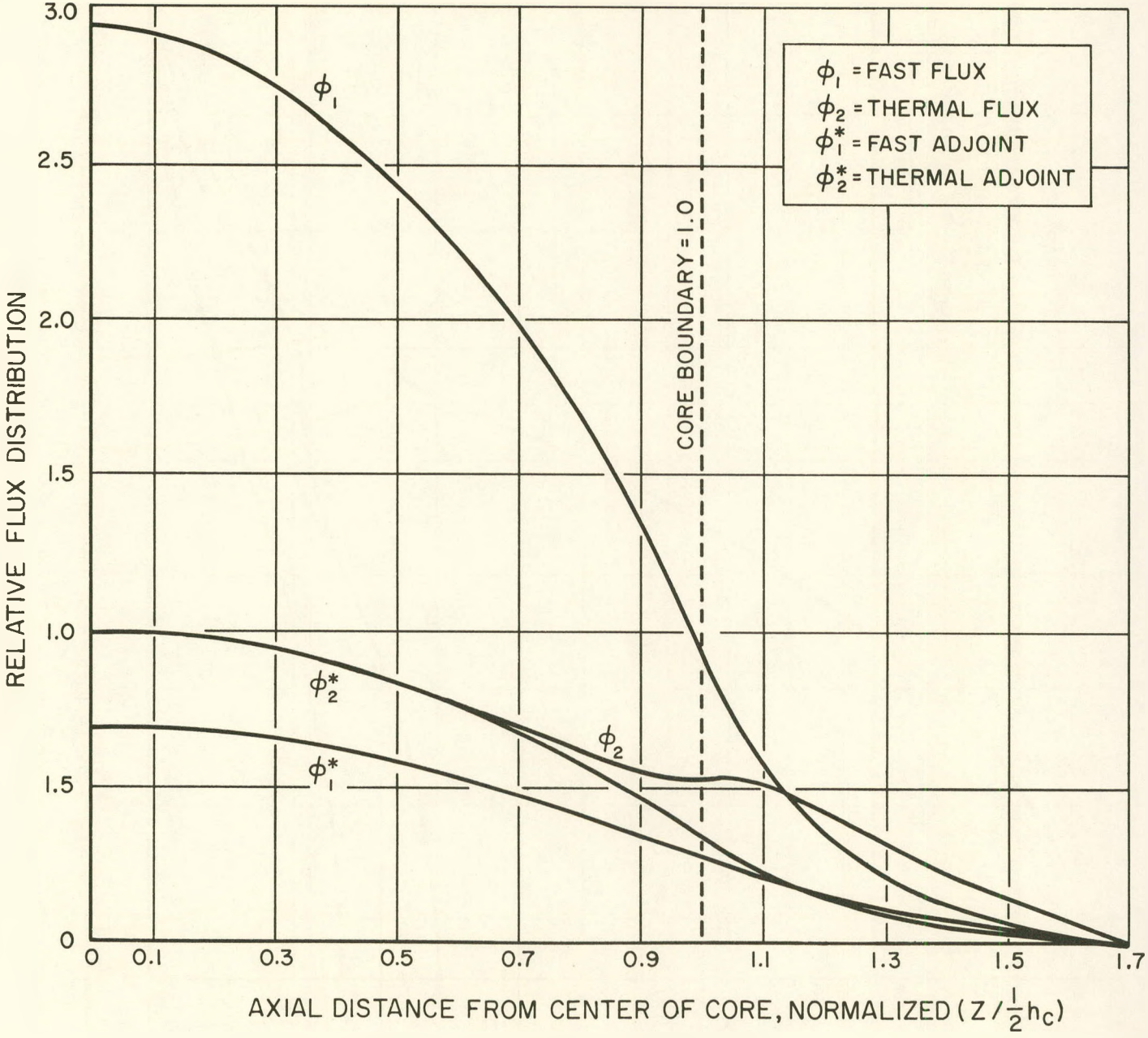

Figure 6. Axial Flux for Wet Case

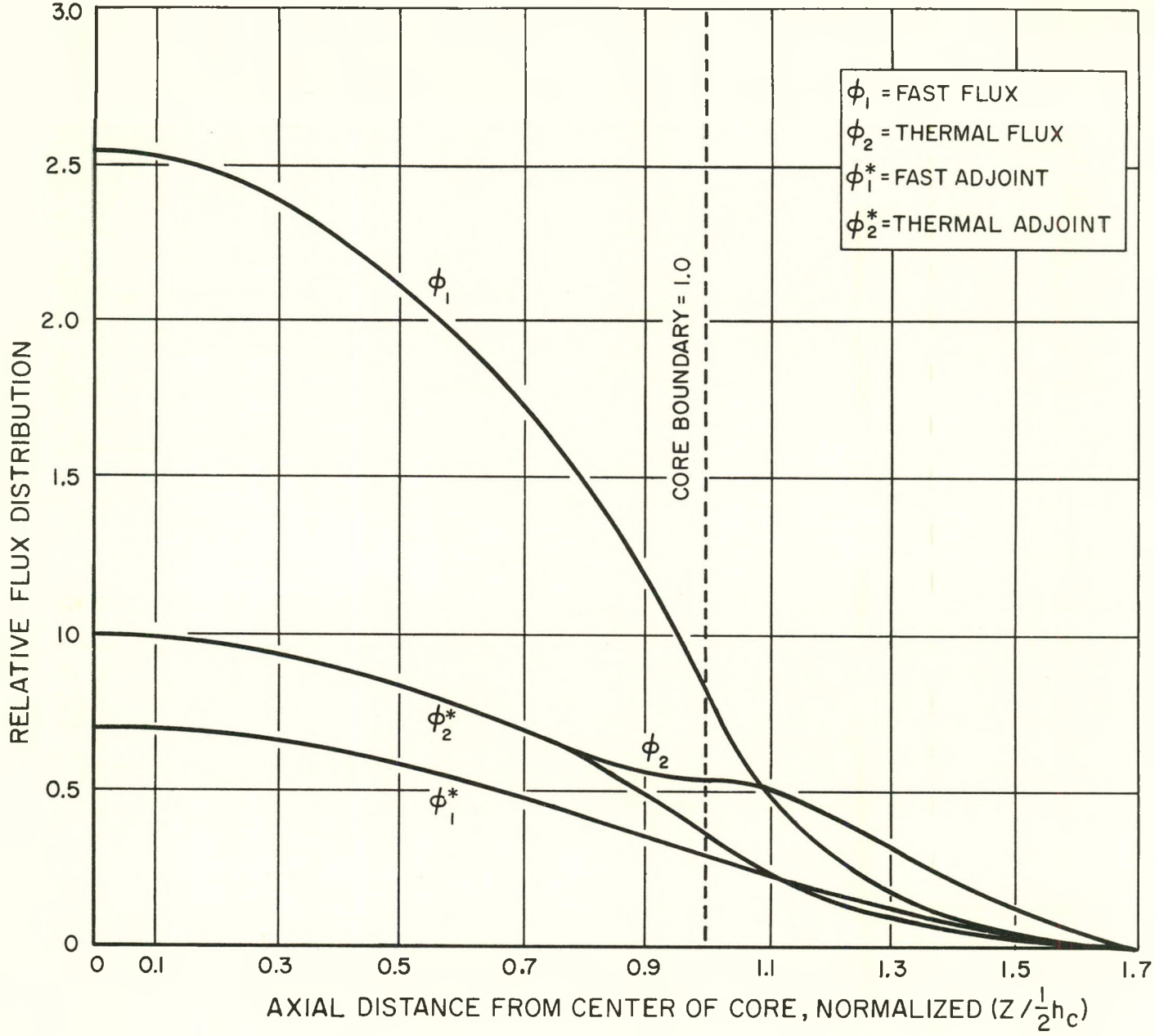

Figure 7. Axial Flux Plot for Hot Case

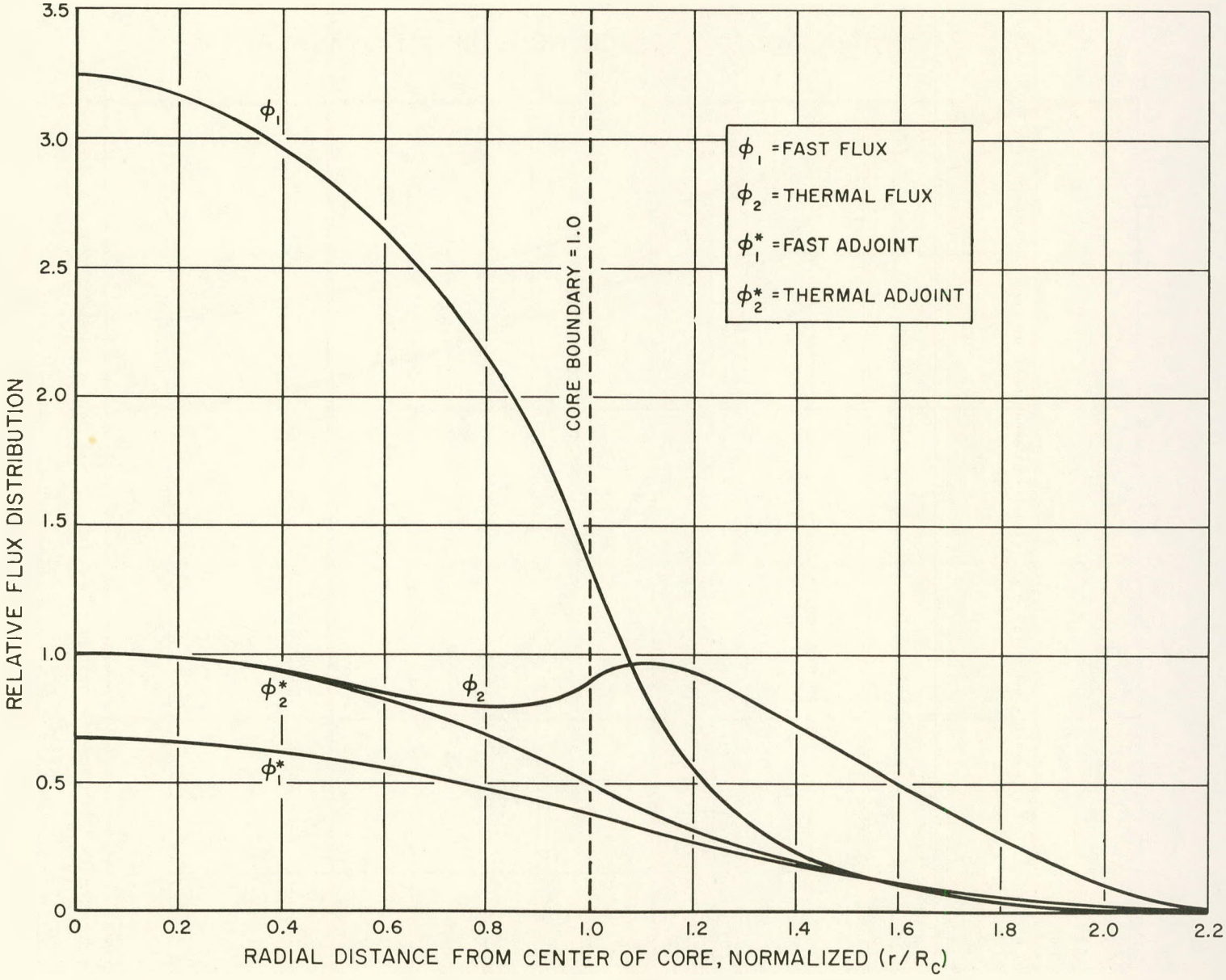

Figure 8. Radial Flux Plot for Dry Case

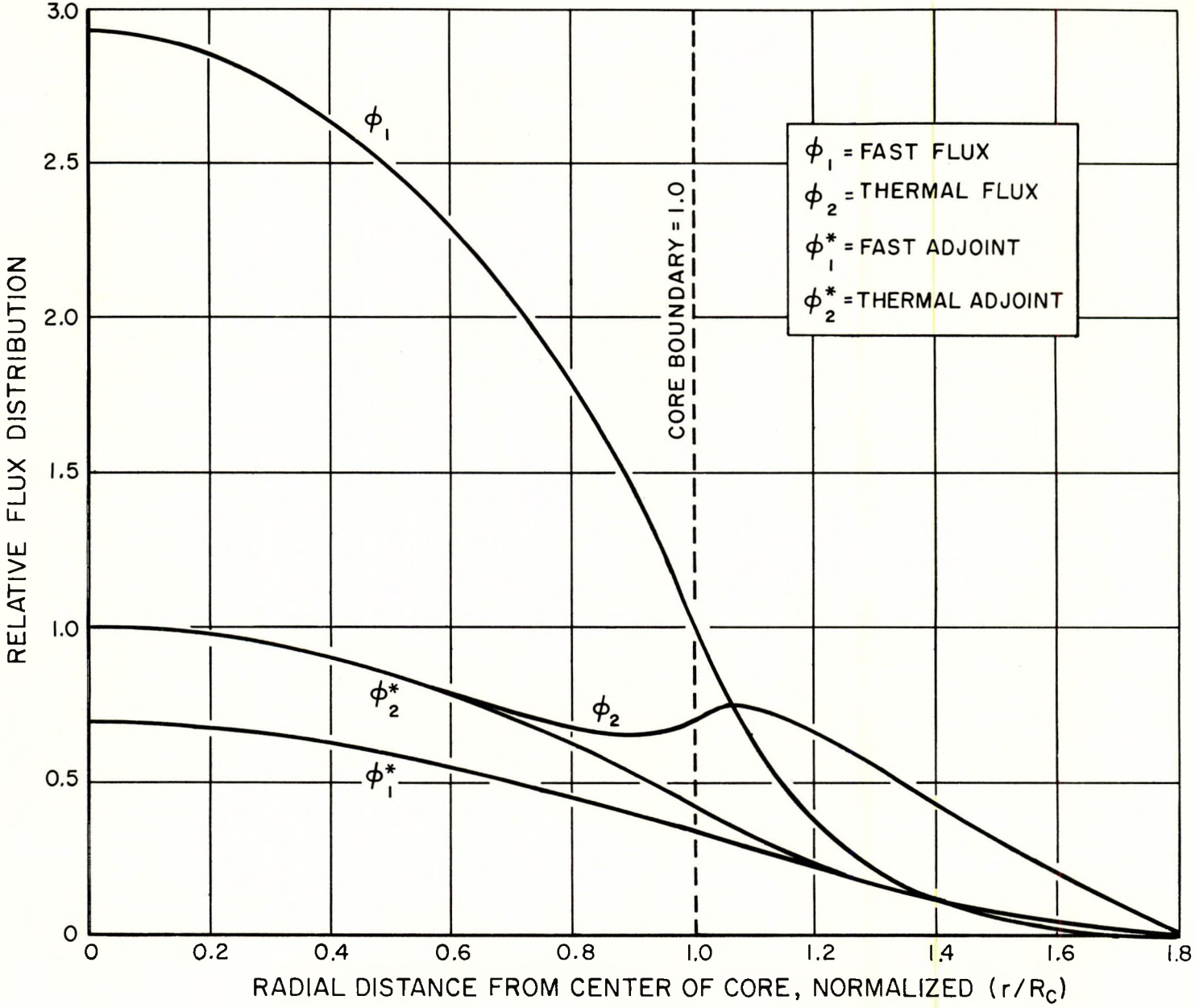

Figure 9. Radial Flux Plot for Wet Case

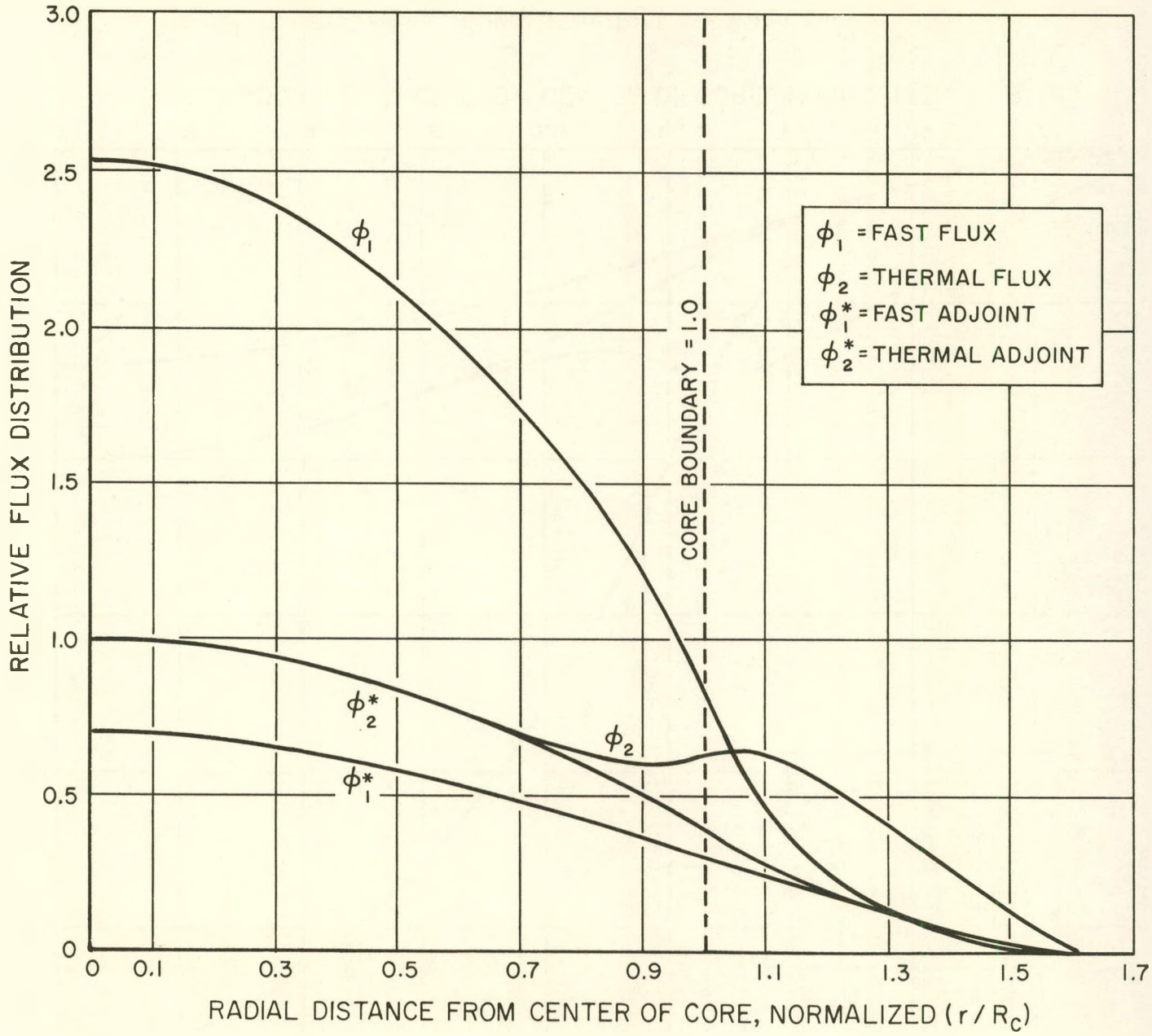

Figure 10. Radial Flux Plot for Hot Case

IX. SUMMARY

The critical masses for three conditions of the SRE reactor have been calculated by two-group theory. The value used for the effective resonance integral of uranium-238 was deduced from exponential experiments having the same fuel cluster and a similar lattice structure to that of the SRE reactor. The thermal flux distribution in a lattice cell was obtained by making an empirical adjustment to the results of a diffusion theory calculation. The adjustment was determined by comparing the cell flux distributions measured in the exponential assemblies with the distribution that the diffusion theory model predicted for these assemblies. The calculated critical masses for the dry and wet reactor conditions were 14.9 percent and 11.9 percent higher, respectively, than the measured values.[10] An accurate critical mass measurement for the hot case is not available.

Several factors influence the reliability of the critical mass calculations described in this report. Of major importance are the geometrical uncertainties pertaining to the reactor structure and the approximations used to reduce complex geometrical shapes to ones which can easily be evaluated. The uncertainties in the value of the uranium-238 resonance integral and in the thermal flux distribution in a lattice cell are two other important factors. Except for these two quantities, the same values were used for basic nuclear properties in both the SRE critical mass calculations and the analysis of the exponential experiments. Consequently, it is expected that uncertainty in the values used for these properties has a relatively minor influence on the reliability of the critical mass calculations. Table XVI lists the major uncertainties which influence the critical mass results, together with an estimate of the magnitude of the contribution of each factor.

Epithermal fission and capture is not included in the two-group method used in these calculations. This effect is undoubtedly even more important in the SRE reactor than it is in the exponential assemblies. Because of the increased neutron spectral hardening caused by the presence of iron, sodium, and zirconium, a larger fraction of the neutrons in SRE will be captured at energies above thermal. Moreover, the inclusion of resonance capture in zirconium and iron will increase the capture above thermal. It has been estimated that resonance integrals of

TABLE XVI

SUMMARY OF FACTORS INFLUENCING THE RELIABILITY OF THE SRE CALCULATIONS

Factor	Uncertainity (percent)	Effect on Critical Mass (percent)
Thickness of sodium layer between moderator cans	10	7.3
Axial reflector properties	10	3.0
Effective resonance integral	10	8.3
Average values of thermal flux in cell	2	3.7

0.6 and 1.1 barns for zirconium and iron, respectively, would increase the calculated critical mass of the dry reactor by about 7 percent. Conversely, the inclusion of epithermal fission will reduce the calculated critical mass. Preliminary calculations indicate that the reduction is substantial.

REFERENCES

1. C. Starr and R. W. Dickinson, Sodium Graphite Reactors (Reading, Mass: Addison-Wesley Publishing Co., Inc. 1958).

2. D. J. Hughes and J. A. Harvey, "Neutron Cross Sections," (Brookhaven National Laboratories, Upton, New York, 1955), BNL-325.

3. W. W. Brown, F. L. Fillmore, and B. L. Scott, "Exponential Experiments with Graphite Lattices Containing Multirod Slightly Enriched Uranium Fuel Clusters," NAA-SR-3096 (1958).

4. E. R. Cohen, "Standard Cross Sections and Reactor Physics Recipes," NAA-SR-Memo-1231 (1955).

5. G. W. Rodeback, "Temperature Coefficients of Uranium and Throium Resonance Integrals," NAA-SR-1641 (1956).

6. J. E. Garvey, "First Collision Probability in Hollow Cylinders," NAA-SR-Memo 1105 (1954).

7. E. R. Cohen, Nuclear Science and Engineering, 2, 227-245 (1957).

8. D. J. Behren's, "The Effect of Holes in a Reacting Material on the Passage of Neutrons," AERE-T/R103.

9. F. L. Fillmore, "Two-Group Calculations of the Critical Core Size of the SRE Reactor," NAA-SR-1517 (1956).

10. R. W. Campbell, "Low Power Physics Experiments on the Sodium Reactor Experiment," NAA-SR-3341 (1959).